Kent Academic Repository

Full text document (pdf)

Citation for published version

Kress, Bernard C. and Osten, Wolfgang and Urbach, H. Paul and Everson, Michael and Duma, Virgil-Florin and Dobre, George (2017) Optical power transmission in a polygon mirror-based swept source optical coherence tomography system. In: SPIE Proceedings. SPIE Proceedings, Digital Optical Technologies. Society of Photo-optical Instrumentation Engineers p. 1033520.

DOI

https://doi.org/10.1117/12.2270256

Link to record in KAR

https://kar.kent.ac.uk/62335/

Document Version

Author's Accepted Manuscript

Optical power transmission in a polygon mirror-based swept source optical coherence tomography system

Michael Everson[1,*] Virgil-Florin Duma[2], George Dobre[3]

[1,3] Applied Optics Group (AOG), School of Physical Sciences (SPS), University of Kent, Canterbury, CT2 7NH, UK; [2]3OM Optomechatronics Group, "Aurel Vlaicu" University of Arad, 77 Revolutiei Ave, Arad 310130, Romania; [2]Doctoral School, Polytechnic University of Timisoara, 1 Mihai Viteazu Ave, Timisoara, 300222, Romania; [2]School of Physics, West University of Timisoara, 4 Vasile Parvan Ave, Timisoara, 300223, Romania

ABSTRACT

Swept Source Optical Coherence Tomography (SS-OCT) relies on the rapid tuning of a broadband light source to produce narrow laser linewidths. Imaging speed is governed by the sweeping frequency of the source and the axial resolution is given by the total bandwidth generated. Mechanical, free space methods, employing rotating polygonal mirrors with a pair of telescopically arranged lenses, can achieve tuning speeds in excess of 100 kHz. Their success relies upon maximising the light throughput of the swept spectrum by reducing the effects of aberration and vignetting caused by the lens design and the geometrical properties of the polygon respectively. However, these properties impose constrictions on the spectral filter's design and care must be taken when building the filter to avoid unnecessarily limiting the performance of the system. This paper presents some of the initial stages of a much larger study into the optimisation of such systems.

Theoretical work has been confirmed by experimental observations and compared with ideal simulations for a spectral filter consisting of a dispersive element, a double lens telescope, arranged in a Littman configuration, and a 72-facet, off-axis polygon mirror with end reflector. A non-linear relationship between the linewidth's location on the telescope in time with the rotation of the polygon was observed and a first approximation for the tuned wavelength with respect to the polygon rotation angle was found. These observations, coupled with ongoing research, will lead to a complete description of polygon based scanners and how their performance can be optimised in future designs.

Keywords: Polygon, OCT, Swept Source, Telescope, Zemax, Spectral Filter, Simulation, Scanning Function.

1. INTRODUCTION

Free space swept sources using a polygonal mirror as a wavelength scanner have been demonstrated successfully in recent years in OCT systems[1,2,3]. Their architecture relies on components that are key to their operation, such as a semiconductor optical amplifier, the polygon mirror itself and an end reflector to guide the light back into the SOA. A dispersive component such as a diffraction grating is also necessary to spatially separate the spectrum into its component wavelengths. A telescope consisting of two lenses is generally used to bring together diffracted beams on the polygon facet[3,4]. The telescope collimates the spatially separated spectrum and directs the collimated beams onto a single mirrored facet of the polygon. An important consideration in the design of such telescopic configurations is on maximising the light throughput between the grating and the end reflector[6,7,8], which in turn provides the required optical power needed at the input of the coherence imaging system.

The propagation of light through the real telescope is characterised by various aberrations, which generally have detrimental effects on the source linewidth, and on the coherence imaging system's resolution and depth penetration[13].

Understanding and quantifying the effects of the parameters of the variable geometries allowed by the particular size and shape of the polygon allows the designer to establish their impact on the system's performance, thus helping improve the line throughput and source linewidth. This is a valuable exercise in optimising swept source configurations using a polygonal wavelength scanner and understanding how to achieve an optimal setup based on given design constraints.

---

*mje23@kent.ac.uk; phone 01227 82 3288; aogkent.uk

In designing a polygon based telescopic spectral filter in Littman configuration[15] from the ground up, a fundamental set of constraints is determined by the choice of polygon geometry (i.e. radius and number of facets). This sets limits on both the numerical exit aperture of the telescope[14] and the beam diameter at the facet. A secondary set of constraints is imposed by the choice of groove density (grating constant) of the diffraction grating, since the angular spread of light towards the first lens of the telescope needs to be fully accommodated. Increasing the focal length of the first lens results in the need to increase the diameter of both lenses (since the propagation of chief rays is parallel to the optical axis). The polygon facet receiving the light from the second lens has a limited acceptance angle due to its limited rotation angle so that is the primary factor that determines the numerical aperture of the lens, and hence its focal length. In both cases care must be taken to specify lens diameters that can accommodate the extra beam width associated with the marginal wavelengths at λ_{min} and λ_{max}. The constraint set by the polygon on the beam width exiting from the telescope is imposed by the size of the facets as this should not be larger than the size of a single facet or else it will introduce vignetting and therefore a loss in power transmission[13]. The polygon facet can be regarded as the optical stop, or limiting aperture (albeit angle dependent), for further propagation.

In this paper, we present a short study of one of the parameters and how it will contribute to a full description of any telescopic, polygon based swept source, arranged in a Littman configuration using a diffraction grating. We have chosen to present theoretically, experimentally and via simulation, the analysis of the lateral displacement (height, h) of the incident wavelength's chief rays on the first lens (L1) and how this will lead towards a complete description of polygon based swept sources. By considering the optimisation of key parameters of a polygon scanner, such as maximising the total power transmission and minimising the laser linewidth, our study consists of resolving the relationships between its components fundamental features and using them to build towards a complete description of the system, whereby these features could determine the overall performance of the system and be modified to achieve full optimisation.

Our set-up, based on previously reported ones[13], relies on the convergence of multiple collimated beams on a polygon facet, each carrying light of a different wavelength and each propagating at a different angle, as shown in Figure 1.
The light source is generated by a Semiconductor Optical Amplifier (SOA) (Covega BOA1017, 600mA) operating with a central wavelength of 1332.8 nm and an initial bandwidth of 75.8 nm. The light is sent via an optical fibre circulator to a collimator, which directs the light onto a transmission grating (Wasatch, 1310 nm, incident angle = 47°, 1145 lines/mm). The dispersed spectrum from the grating is captured by a telescope, consisting of two lenses, L1 and L2, (Thorlabs AC254-075-C and AC254-100-C), which focus the beams onto a single facet of the polygon mirror (SA34 Lincoln Laser, radius = 31.75 mm, 72 facets, 5°/facet, 2.77 mm x 6.35 mm facet size). An off-axis design is chosen to double the size of the acceptance angle of the polygon and therefore decrease the laser linewidth by increasing the sweeping range[6,8,9,10]. The off-axis design requires an end reflector mirror to retroreflect the individual linewidths, in sequence, back through the system of components where it is recaptured by the collimator and subsequently circulated through the SOA for amplification before exiting the filter via a fibre coupler and sent to the coherence imaging system.
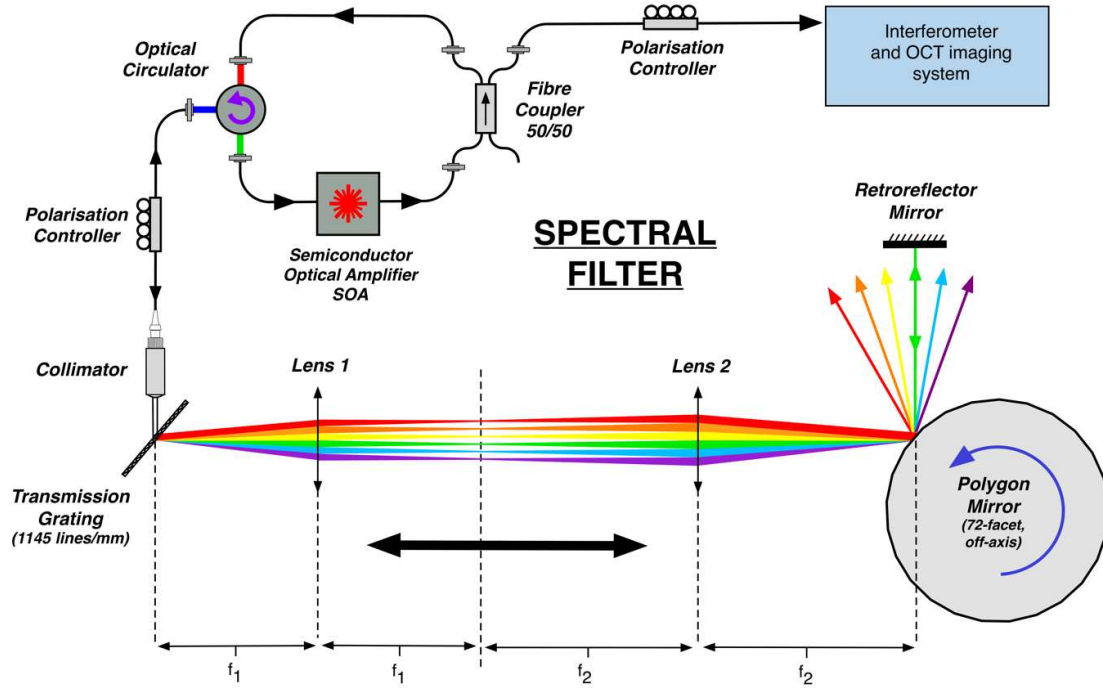
Figure 1. Spectral filter consisting of a semiconductor optical amplifier (SOA), optical circulator, collimator, transmission grating, two lens telescope, polygon mirror and retroreflector mirror. After filtering the light is circulated through the amplifier and coupled off towards the OCT imaging system.

2. THEORETICAL ANALYSIS

Considerations were given to the diffraction gratings operation and the y-coordinate (which we denote h) of the chief ray for any given wavelength, λ, incident on L1. The lateral displacement or height, h, of each of the wavelength's chief rays was determined through a purely geometrical analysis. The central wavelength, $\lambda_c = 1332.8\ nm$, was chosen to coincide with the optical axis making the height on L1, $h = 0\ mm$. This provides a coordinate system in the y, z plane only. The optical axis (z) sits at h = 0. Therefore, the height, h, has both positive and negative values for any given wavelength location on L1. Knowing the overall lateral displacement of the swept spectrum on the lens provides the first steps towards knowing its location in time and how this might be minimised, since higher scanning speeds improve the quality of the final imaging system.

First, to find the height, h, on L1, the grating equation must be rearranged to give the diffraction angle as a function of wavelength, $\delta(\lambda)$

$$\delta(\lambda) = \sin^{-1}(Gm\lambda - \sin\gamma) \tag{1}$$

where G is the grating constant (1145 lines per mm), m is the diffraction order ($m = 1$ only) and γ is the angle of incidence on the grating (47 degrees) given by the specifications of our chosen component.

Each wavelength, λ_n, exits the grating at an angle $\alpha_n = \delta_n - \delta_c$ from the optical axis, where δ_n is the diffraction angle of λ_n and δ_c is the diffraction angle of the central wavelength, $\lambda_c = 1332.8\ nm$ (see fig. 2).
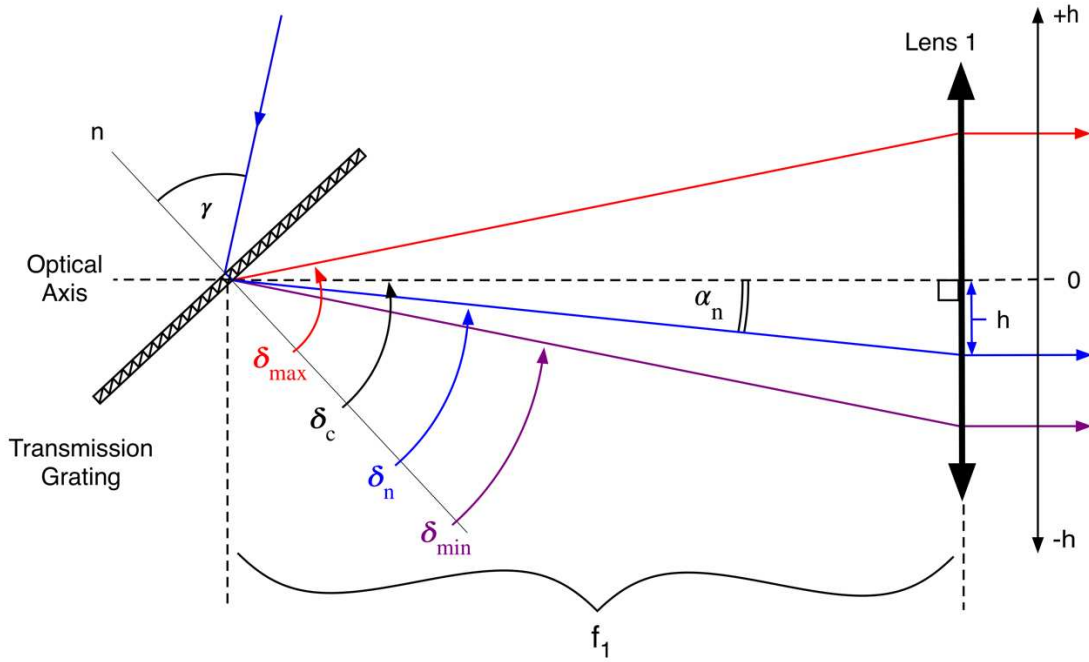
Figure 2. The diagram depicts the propagation of light between the grating and lens 1 (L1). If the spectrum of light incident on the grating is sampled at a coordinate λ_n, then the diffraction angle, δ_n, is given as a function of wavelength, $\delta(\lambda_n)$.

This ensures a positive and negative height respectively on the upper and lower side of the optical axis. Taking the product of the focal length and the tangent of α_n gives the height on L1.

$$h_1(\delta_n) = f_1 \tan(\delta_n - \delta_c) \tag{2}$$

Substituting the grating equation for $\delta_n(\lambda_n)$ and $\delta_c(\lambda_c)$ gives the height as a function of wavelength.

$$h_1(\lambda_n) = f_1 \tan[\sin^{-1}(Gm\lambda_n - \sin\gamma) - \sin^{-1}(Gm\lambda_c - \sin\gamma)] \tag{3}$$

Equation 1.3 provides a starting point for a full description of the height of the chief ray for a chosen wavelength, λ_n, at any instant in time relative to the rotation of a single facet of the polygon. This was then compared with our simulation and finally verified experimentally.

3. SIMULATED ANALYSIS

Simulations were carried out using Zemax™ Ray Tracing Software to compare with the theoretical and experimental findings at each step of the analysis (Fig. 3). We produced an ideal setup using paraxial lenses that suffer no aberration effects. The simulation could be set up to replicate the experimental apparatus in its entirety including the single mode fibre output that the light originates and returns to, which is essential for understanding the light throughput of the system. To simulate the bandwidth, 11 equidistantly spaced wavelengths, λ_n, centred at 1332.8 nm over a bandwidth of 125 nm, were set up to traverse through the system. Each wavelength requires its own configuration whereby the polygon's rotation angle must be set to reflect the light at normal incidence off the retroreflector mirror. The angle on the polygon for each wavelength was adjusted until the maximum amount of light was received back into the single mode fibre. The angle was measured in degrees and required tuning down to the 4th decimal place.
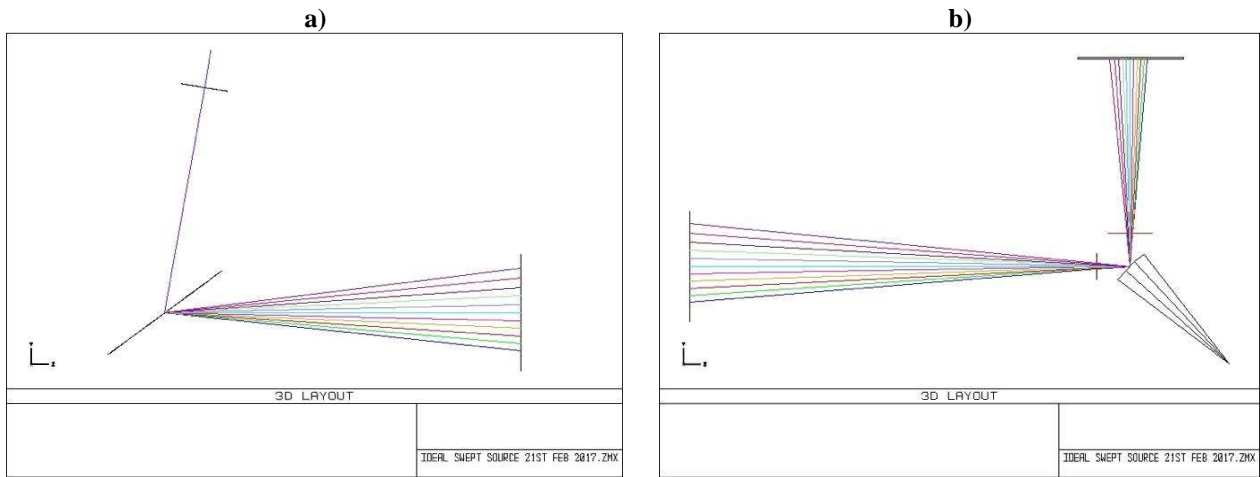
Figure 3. The 3D layout from the simulation. Starting in the top left and listed in sequence; **a)** Optical Fibre (9 μm), Paraxial Collimator Lens, Diffraction Grating and Paraxial Lens 1. All 11 wavelengths can be seen exiting the grating and terminating on the first lens. **b)** Paraxial Lens 2, Polygon Mirror and Retroreflector Mirror. At 45 degrees, only the central wavelength is reflected off the retroreflector mirror at normal incidence and sent back to the fibre.

With the central wavelength propagating along the optical axis, the height on L1 could be found by reading off the y-coordinate for each of the wavelength's chief rays in the spectrum. Footprint diagrams were also used to display the spot of each wavelength's beam and its location on the lens.

a) Footprint diagram on Lens 1
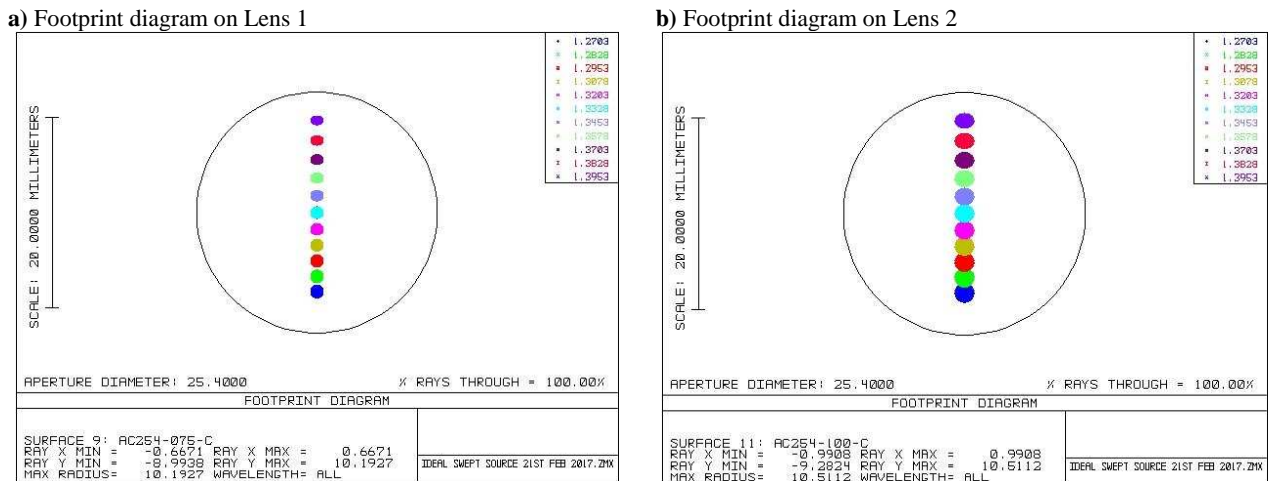
b) Footprint diagram on Lens 2

Figure 4. Footprint diagrams of the 11 incident beams on both lenses in the x, y plane. Note the change in shape of the beams with increasing wavelength and the increased size on L2 due to the ratio of their focal lengths. More interestingly, their spatial distribution decreases with increasing wavelength, suggesting a non-linear relationship between their location in time with the rotation of the polygon.

The analysis shows a change in the spot size from the first lens to the second and a change in shape from a circular to elliptical as the wavelength increases. This is, as expected, from the ratio of the different focal lengths impacting upon the beam width. The size in the x-direction remains constant over the spectrum (as expected) but the size in the y-direction becomes narrower with increasing wavelength, which corresponds to an increasing diffraction angle off the transmission grating and therefore a larger incident angle on the lens. We also see that the beams are more tightly spaced towards the shorter wavelengths, which overlap by the time they reach the second lens, suggesting that the spectrum has a higher energy density over the shorter wavelengths and therefore will have a non-linear relationship between the filtered spectrum and the rotation of the polygon.

4. EXPERIMENTAL ANALYSIS

To verify the theoretical study, light from a collimator was captured, after passing through the first lens, and fed into a spectrum analyser (Fig. 5). The collimator was aligned with the optical axis and the height was measured using a translation stage with a resolution of 10 microns. The collimator and its stage were adjusted simultaneously until the power transmission was maximised and the central wavelength of 1332.8 nm was found. The reading on the micrometre was then recorded and used to zero its location in order to be easily comparable with the values given by the theory. 13 measurements were recorded over the 0-12 mm range of the translation stage whereby the wavelength and its associated power were recorded for each position. We assume that the transmission grating and the lens are perfectly aligned with each other and that the central wavelength lies exactly along the optical axis of the telescope. The translation stage is also assumed to operate at exactly 90 degrees to the optical axis. Any continuous deviations from the expected values can be attributed to tiny departures from this assumption.
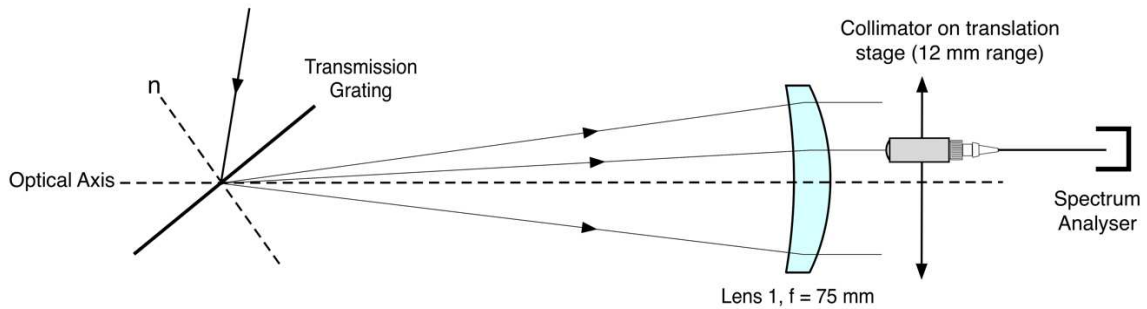

Figure 5. Experimental setup for measuring the height of each wavelength on the first lens.

To compare the results, new theoretical values were calculated, using equation 1.3, for each of the 13 wavelengths recorded in the experiment.
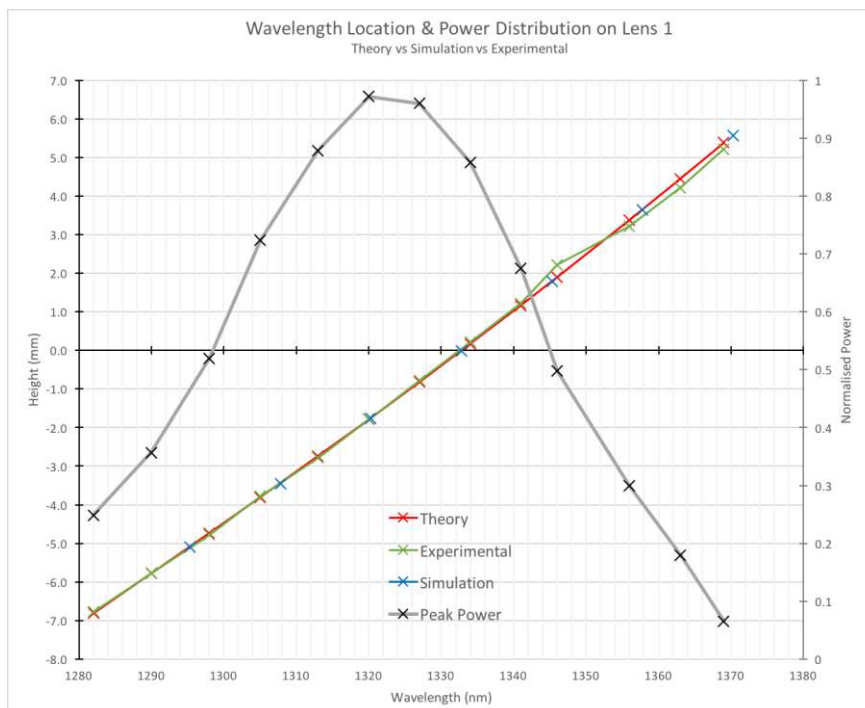

Figure 6. Comparison between theoretical, simulated and experimental results for the height, h, on lens L1 as well as the normalised power received for each wavelength measurement.

The graph in figure 6 provides a comparison between theory, simulation and experiment, and demonstrates that they are in good agreement with each other. Slight deviations are noticed on the experimental values toward the longer wavelengths, which can be explained by the non-linear separation distances (nanometers) between each of the observed wavelengths in the experiment (see fig. 7). The power measured on the spectrum analyser for each wavelength is also shown on the same graph. This shows a bell curve with its peak shifted slightly towards the shorter wavelengths in the spectrum, confirming the earlier observation that the spatial distribution of the spectrum has an uneven distribution, with a higher density towards the shorter wavelengths.
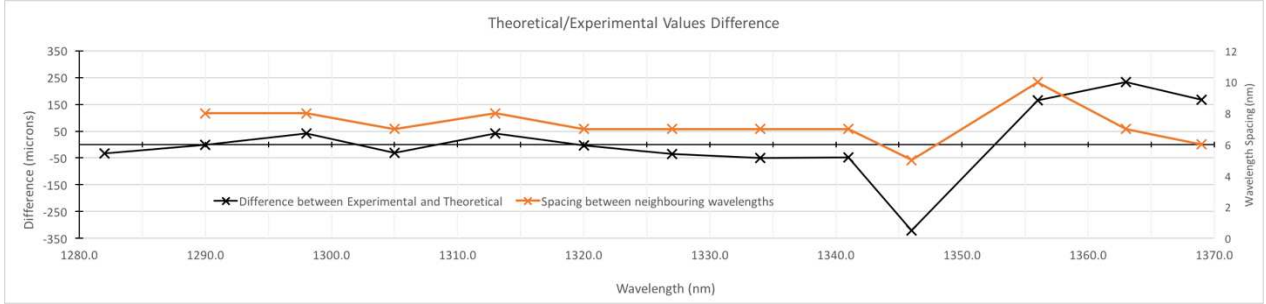

Figure 7. The difference (in microns) between the theoretical and experimental height (black) plus the separation (in nanometers) between adjacent wavelengths (orange). The trend of both curves match one another, providing an explanation for the deviation seen at the end of the spectrum.

Figure 7 gives the difference in microns between the theoretical and the experimental values. The largest deviation, at approximately 320 microns, is supported by the fact that the separation between adjacent wavelengths was not linear.

5. THE SCANNING FUNCTION

A recent study on the effect of capturing light through a lens after reflection off a rotating polygon mirror produced theoretical predictions for the height of the beam on the lens with respect to the rotation angle of the polygon[14]. The analysis was carried out purely from observations of the polygon system's geometry, and this study's theoretical results are verified experimentally in our present study. An expression called the scanning function that depends only upon the parameters of the polygon and its arrangement, which was also set up off-axis with the incident beam propagating onto the polygon with an incidence angle of 45°. This is effectively identical to the return path of our setup, starting at the retroreflector mirror and sequentially reflecting off the polygon and through the second lens (see fig. 1 & fig. 3, b)).

The scanning function, consisting of five terms, is given as a function of the polygons radius, R, the eccentricity, e (owing to the off-axis design), and the distance, L, of the lens from the polygons facet (in our case this is the focal length of the second lens).

$$h(\theta) = R\sqrt{2} - e - \frac{R}{\cos\theta} + e \cdot \tan\theta - \frac{L}{\tan 2\theta} \tag{4}$$

Where θ is the rotation angle of the polygon, which has a restricted range depending on the number of facets used. In our setup, θ has a range of 5° due to the fact that the angle per facet is $2\pi/n$, where $n = 72$. Using the values in our setup (R = 31.75 mm, e = 22.45 mm, L = f$_2$ = 100 mm), we can plot the scanning function over an appropriate range ($42.5° \leq \theta \leq 47.5°$). The values recorded in our simulation, the polygon angle and the height of each wavelength on the lens, can also be inserted into the graph for comparison.
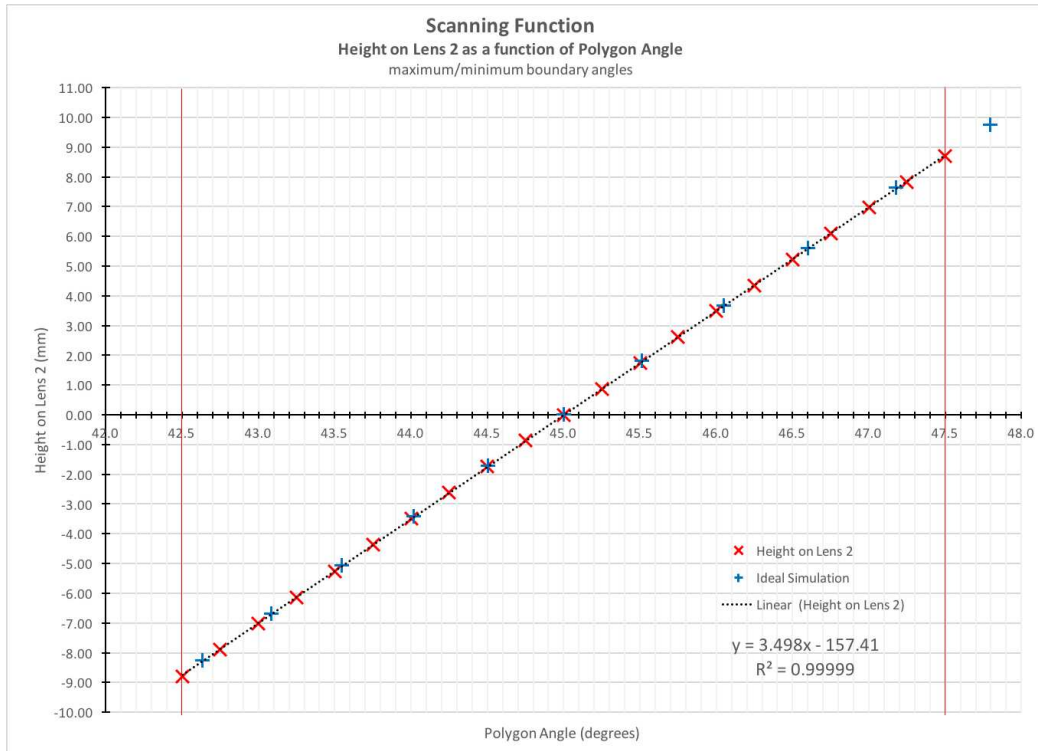
Figure 8. Over such a short range of angles, the curve produced by the scanning function takes on a linear trend. The red bars show the limit of the polygons rotation angle due to the number of degrees per facet. Our largest wavelength in the simulation falls outside this range and therefore will not become part of the swept spectrum that is sent to the imaging system. This is also seen in our simulations (see fig. 9).

Since an adjacent facet becomes active after 5° of polygon rotation, the graph in figure 8 has been issued with boundary markers at the appropriate locations, centred on 45°. The longest wavelength used in our simulation is shown outside of these markers and therefore does not contribute to the swept spectrum in the imaging system. This is further confirmed by observing the 3D layout images from the simulations (fig. 9).
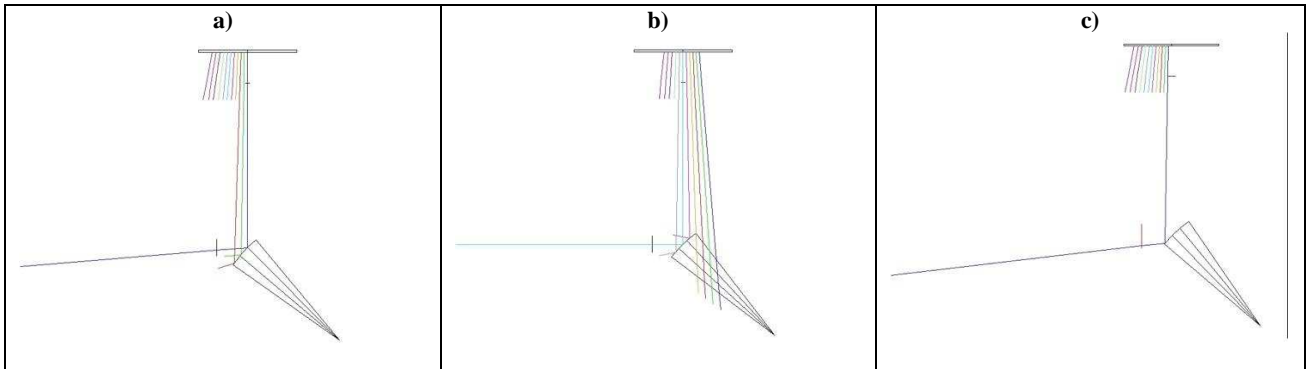

Figure 9. Propagation of light of three chosen wavelengths from the reflecting mirror, showing chief rays originating on the retroreflector mirror and terminating on the second lens. Only the correct polygon angle for each incident ray will propagate exactly in reverse along the path it travelled, allowing it to be captured in the single mode fibre. Configuration 1 (a) (1270.3 nm @ 42.6299 degrees) shows the chief ray only just striking the correct facet while configuration 11 (c) (1395.3 nm @ 47.7968 degrees) shows the chief ray striking the adjacent facet, below the target facet, which causes the ray to propagate towards the second lens at the wrong angle. Configuration 6 (b) (1332.8 nm @ 44.9998 degrees) shows the chief ray reflecting exactly along the optical axis of the system from the centre of the target facet.

The curve in the graph is tangential by nature but approximates to a straight line over the short range of angles being used. From the trend line, we can extract the linear equation for $h(\theta)$ and rearrange it to give $\theta(h)$.

$$\theta(h) = \frac{h + 157.41}{3.498} \tag{5}$$

If we then substitute our own equation for $h(\lambda)$ (Eq. 3) we obtain $\theta(\lambda)$.

$$\theta(\lambda_n) = \frac{f_1 \tan[\sin^{-1}(Gm\lambda_n - \sin\gamma) - \sin^{-1}(Gm\lambda_c - \sin\gamma)] + 157.41}{3.498} \tag{6}$$

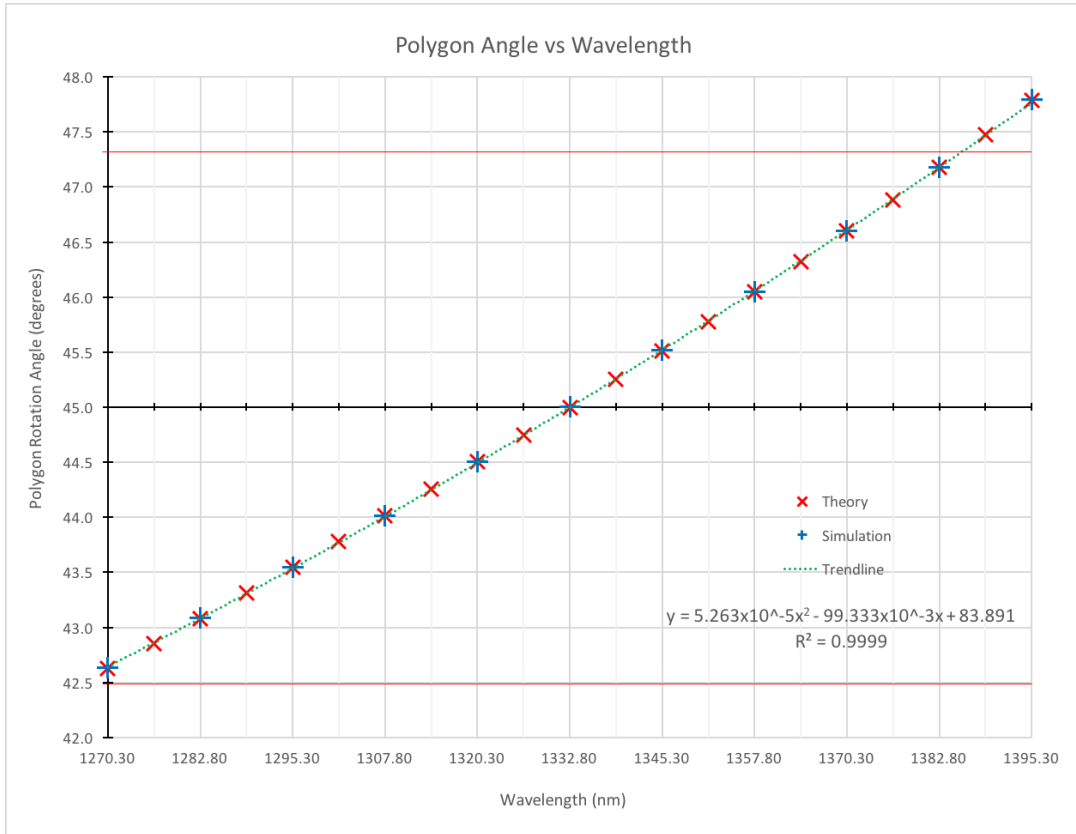We can now plot the graph of polygon angle as a function of wavelength.

Figure 10. Polygon rotation angle, θ, required by each wavelength for optimal reinjection into the single mode fibre.

We see that the spectrum is clipped at the longest wavelengths, which is indicated by the final markers laying beyond the boundary of 47.5 degrees.

The polynomial trend line of the curve in Figure 10 is given as

$$\theta(\lambda) = 5.263 \times 10^{-5} \cdot \lambda^2 - 99.333 \times 10^{-3} \cdot \lambda + 83.891 \tag{7}$$

This allows for an expression of $\lambda(\theta)$ with numerical coefficients to be developed:

$$\lambda(\theta) = \sqrt{1.9 \times 10^4 \cdot \theta - 7.0 \times 10^5} + 9.4 \times 10^2 \tag{8}$$

6. CONCLUSION

For any given wavelength λ_n we have studied the chief ray intercept at the principal plane of the lens L1, comparing it with our simulation and verifying it experimentally. Very good agreement was observed between the three modalities. We have further obtained a relationship between θ and λ, where θ is the required polygon angle for maximum reinjection of light of an instantaneous wavelength λ.

We have shown that by using a diffractive element (in our case a transmission grating) the footprint of the dispersed beam undergoes a narrowing in the y-direction with increasing wavelength, and the footprint itself becomes more elliptical in shape as the diffraction angle after the transmission grating increases.

This footprint variation has important implications for the eventual vignetting that these beams are expected to undergo at the polygon facet, since the narrower beams are less susceptible to vignetting. One interesting implication is for the siting of the polygon in relation to the optical axis, which we are investigating further.

The spacing of the energy density towards the shorter wavelengths points towards a non-linear relationship between the filtered spectrum and the rotation of the polygon. This in turn implies a nonlinear dependence of wavelength against time in the swept spectrum.

The expression for $\lambda(\theta)$ is an important step along the path that leads towards an expression for the power spectral density of light that is reinjected into the fibre, and therefore towards the instantaneous linewidth of the spectral filter.

It is important to note that our analysis, while numerical in nature, was carried out with the assumption of a 5 degree facet sweep angle polygon, and further research we are conducting will extend this study to a variety of polygon geometries.

ACKNOWLEDGEMENTS

REFERANCES

[1] Bräuer, B., Lippok, N., Murdoch, S.G. and Vanholsbeeck, F., "Simple and versatile long range swept source for optical coherence tomography applications", Journal of Optics, **17(12)**, pp.125301, (2015).

[2] Kwon, Y.S., Ko, M.O., Jung, M.S., Park, I.G., Kim, N., Han, S.P., Ryu, H.C., Park, K.H. and Jeon, M.Y., "Dynamic sensor interrogation using wavelength-swept laser with a polygon-scanner-based wavelength filter", Sensors, **13(8)**, pp.9669-9678. (2013)

[3] Motaghiannezam, S.R., Koos, D. and Fraser, S.E., "Differential phase-contrast, swept-source optical coherence tomography at 1060 nm for in vivo human retinal and choroidal vasculature visualization". Journal of biomedical optics, **17(2)**, pp.0260111-0260115. (2012).

[4] Lee, K.K., Mariampillai, A., Joe, X.Z., Cadotte, D.W., Wilson, B.C., Standish, B.A. and Yang, V.X., "Real-time speckle variance swept-source optical coherence tomography using a graphics processing unit". Biomedical optics express, **3(7)**, pp.1557-1564. (2012).

[5] Lee, S.W., Song, H.W., Jung, M.Y. and Kim, S.H., "Wide tuning range wavelength-swept laser with a single SOA at 1020 nm for ultrahigh resolution Fourier-domain optical coherence tomography". Optics express, **19(22)**, pp.21227-21237. (2011).

[6] Oh, W.Y., Vakoc, B.J., Shishkov, M., Tearney, G.J. and Bouma, B.E., "> 400 kHz repetition rate wavelength-swept laser and application to high-speed optical frequency domain imaging". Optics letters, **35(17)**, pp.2919-2921. (2010).

[7] Al-Qaisi, M.K. and Akkin, T., "Swept-source polarization-sensitive optical coherence tomography based on polarization-maintaining fiber". Optics express, **18(4)**, pp.3392-3403. (2010).

[8] Mao, Y., Flueraru, C., Sherif, S. and Chang, S., "High performance wavelength-swept laser with mode-locking technique for optical coherence tomography". Optics Communications, **282(1)**, pp.88-92. (2009).

[9] Liu, G.Y., Mariampillai, A., Standish, B.A., Munce, N.R., Gu, X. and Vitkin, I.A., "High power wavelength linearly swept mode locked fiber laser for OCT imaging". Optics express, **16(18)**, pp.14095-14105. (2008).

[10] Lee, E.C., de Boer, J.F., Mujat, M., Lim, H. and Yun, S.H., "In vivo optical frequency domain imaging of human retina and choroid". Optics Express, **14(10)**, pp.4403-4411. (2006).

[11] Oh, W.Y., Yun, S.H., Tearney, G.J. and Bouma, B.E., "115 kHz tuning repetition rate ultrahigh-speed wavelength-swept semiconductor laser". Optics letters, **30(23)**, pp.3159-316. (2005).

[12] Yun, S.H., Boudoux, C., Tearney, G.J. and Bouma, B.E., "High-speed wavelength-swept semiconductor laser with a polygon-scanner-based wavelength filter". Optics letters, **28(20)**, pp.1981-1983. (2003).

[13] Everson, M., Duma, V.F. and Dobre, G., "Geometric & radiometric vignetting associated with a 72-facet, off-axis, polygon mirror for swept source optical coherence tomography (SS-OCT)", AIP Conference Proceedings, **1796(1)**, pp. 040004. AIP Publishing (2017).

[14] Duma, V.F, "Polygonal mirror laser scanning heads: Characteristic functions", PROCEEDINGS OF THE ROMANIAN ACADEMY SERIES A-MATHEMATICS PHYSICS TECHNICAL SCIENCES INFORMATION SCIENCE, **18(1)**, pp. 25-33. (2017).

[15] Liu, K. and Littman, M.G., "Novel geometry for single-mode scanning of tunable lasers". Optics Letters, **6(3)**, pp.117-118. (1981).